Mon. Not. R. Astron. Soc. **000**, 1–9 (2009) Printed 1 June 2009 (MN LATEX style file v2.2)

Gas in Simulations of High Redshift Galaxies and Minihalos

Smadar Naoz[1⋆], Rennan Barkana[1,2] & Andrei Mesinger[3]†
[1] *Raymond and Beverly Sackler School of Physics and Astronomy, Tel Aviv University, Tel Aviv 69978, Israel*
[2] *Division of Physics, Mathematics and Astronomy, California Institute of Technology, Mail Code 130-33, Pasadena, CA 91125, USA*
[3] *Department of Astrophysical Sciences, Princeton University, Princeton, NJ 08544, USA*

1 June 2009

ABSTRACT
We study the gas content of halos in the early universe using high resolution hydrodynamical simulations. We extract from the simulations and also predict based on linear theory the halo mass for which the enclosed baryon fraction equals half of the mean cosmic fraction. We find a rough agreement between the simulations and the predictions, which suggests that during the high-redshift era before stellar heating, the minimum mass needed for a minihalo to keep most of its baryons throughout its formation was $\sim 3 \times 10^4$ $M_\odot$. We also carry out a detailed resolution analysis and show that in order to determine a halo's gas fraction even to 20% accuracy the halo must be resolved into at least 500 dark matter particles.

Key words: galaxies:high-redshift – cosmology:theory – galaxies:formation

1 INTRODUCTION

The formation of galaxies is one of the most important research areas in cosmology. Within the simplified hierarchical scenario of a universe governed by a cosmological constant and cold dark matter, the density profiles of forming halos have been well characterized (Navarro, Frenk, & White 1997). However, the complex processes of gas dynamics, such as cooling and heating mechanisms, that are responsible for the formation of luminous objects still pose many theoretical difficulties.

Numerical calculations show that the first generation of galaxies formed at very high redshifts inside collapsing halos (starting at $z \sim 65$; Naoz, Noter, & Barkana 2006), corresponding to high peaks of the primordial density field. Indeed, The *Wilkinson Microwave Anisotropy Probe* (*WMAP*) measured a Thomson scattering optical depth of $\tau_e = 0.09 \pm 0.019$ from their 5-year data (Dunkley et al. 2008). When combined with simple analytic perscriptions of the growth of the global ionized fraction (e.g., fig. 22 Barkana & Loeb 2001; Mesinger, Johnson, & Haiman 2006, fig. 9), this measurement suggests that reionization began at very high redshifts, $z \gtrsim 15$. This means that a high enough abundance of luminous objects must have existed at that time, since these first luminous objects are expected to have heated and reionized their surroundings (e.g., Barkana & Loeb 2001; Wyithe & Loeb 2003; Haiman & Holder 2003; Cen 2003).

The formation of a luminous object inside a halo requires, of course, gas to be inside the halo. Even in halos that are too small for cooling via atomic hydrogen, i.e., minihalos, the gas content can have substantial, and observable, astrophysical effects. In addition to the posibility of hosting astrophysical sources, minihalos may produce a 21-cm signature (Kuhlen, Madau, & Montgomery (2006); Shapiro et al. (2006); Naoz & Barkana (2008) but see Furlanetto & Oh (2006)), and they can block ionizing radiation and produce an overall delay in the global progress of reionization (e.g., Barkana & Loeb 2002; Iliev et al. 2003, 2005; McQuinn et al. 2007). Thus, the evolution of the halo gas fraction at various epochs of the universe is of prime importance, particularly in the early universe.

The estimation of the gas fraction in simulations and semi-analytical models has been extensively investigated and used for various purposes (e.g., Efstathiou 1992; Shapiro, Giroux, & Babul 1994; Thoul & Weinberg 1996; Quinn, Katz, & Efstathiou 1996; Hui & Gnedin 1997; Bromm, Coppi, & Larson 1999; Gnedin 2000; Kitayama & Ikeuchi 2000; Abel, Bryan, & Norman 2002; Bromm, Coppi, & Larson 2002; Helly et al. 2003; Bromm & Loeb 2004; Dijkstra et al 2004; O'Shea et al. 2005a; Mesinger, Bryan & Haiman 2006; Naoz & Barkana 2007; Mesinger, Bryan, & Haiman 2008; Trenti & Stiavelli 2009). When investigating this issue with simulations, a large volume is needed for an adequate statistical sample of halos, but on the other hand it is critical to maintain the proper resolution. The results of Springel & Hernquist (2003) showed that in order to determine the mass and

⋆ E-mail: smadar@wise.tau.ac.il
† Hubble Fellow

merger history of each halo even crudely in simulations, each halo must be resolved into 500 particles. In the high redshift regime, where halos are small and rare, these resolution requirements are not easy to achieve. Nonetheless, it is important to do so in order to understand the formation of the first objects.

Consider the various scales involved in the formation of non-linear objects containing DM and gas. On large scales (small wavenumbers) gravity dominates halo formation and gas pressure can be neglected. On small scales, on the other hand, the pressure dominates gravity and prevents baryon density fluctuations from growing together with the dark matter fluctuations. The relative force balance at a given time can be characterized by the Jeans (1928) scale, which is the minimum scale on which a small gas perturbation will grow due to gravity overcoming the pressure gradient. As long as the Compton scattering of the cosmic microwave background (CMB) on the residual free electrons after cosmic recombination kept the gas temperature coupled to that of the CMB, the Jeans mass was constant in time. However, at $z \sim 200$ the gas temperature decoupled from the CMB temperature and the Jeans scale began to decrease with time as the gas cooled adiabatically. Any overdensity on a scale more massive than the Jeans mass at a given time can begin to collapse, due to a lack of sufficient pressure. However, the Jeans mass is related only to the evolution of perturbations at a given time. When the Jeans mass itself varies with time, the overall suppression of the growth of perturbations depends on a time-averaged Jeans mass.

Gnedin & Hui (1998) defined a "filtering mass" that describes the highest mass scale on which the baryonic pressure still manages to suppress the linear baryonic fluctuations significantly. Gnedin (2000) suggested, based on a simulation, that the filtering mass also describes the largest halo mass whose gas content is significantly suppressed compared to the cosmic baryon fraction. The latter mass scale, in general termed the "characteristic mass", is defined as the halo mass for which the enclosed baryon fraction equals half the mean cosmic fraction. Thus, the characteristic mass distinguishes between gas-rich and gas-poor halos. Many semi-analytical models of dwarfs galaxies often use the characteristic mass scale in order to estimate the gas fraction in halos (Bullock, Kravtsov, & Weinberg 2000; Benson et al. 2002a,b; Somerville 2002).Recently, Hoeft et al. (2006) and Okamoto, Gao, & Theuns (2008) showed that the characteristic mass scale does not agree with the Gnedin & Hui (1998) filtering mass in the low-redshift, post-reionization regime.

In this paper we explore the very high-redshift regime using three-dimensional hydrodynamical simulations based on Mesinger, Bryan & Haiman (2006). They investigated the effects of a photo-ionizing ultraviolet (UV) flux on the collapse and cooling of small halos in relic HII regions at high redshift, by varying the strength and duration of a transient UV and persistent Lyman-Werner (LW) background. We consider two different scenarios presented there (see Section 2 for a description of the simulations). We perform a resolution study and place a lower limit on the number of particles needed in a simulated halo in order to accurately determine the gas fraction in halos (Section 3). We also compare the numerical evolution of the filtering mass as given by the linear calculation in Naoz & Barkana (2007) to the simulation results (Section 4). Finally, we summarize and discuss our results in Section 5.

Table 1. Main characteristics of the simulations.

Simulation name	Box size [Mpc/h]	Static refinement levels	Inner refined region [Mpc/h]	$M_{\rm dm}$ [$M_\odot$]
VLres	1	2	0.25	747
Lres	1	3	0.25	93
Hres	0.35	3	0.0875	4.0
VHres	0.25	3	0.0625	1.46

2 THE SIMULATIONS

Our simulations assume the following cosmological parameters: (Ω_Λ, $\Omega_{\rm M}$, Ω_b, n, σ_8, H_0) = (0.7, 0.3, 0.047, 1, 0.92, 70 km s^{-1} Mpc^{-1}). We use the Eulerian adaptive mesh refinement (AMR) code Enzo, which is described in greater detail in Bryan (1999), Norman & Bryan (1999) and Mesinger, Bryan & Haiman (2006). Our simulation volumes are initialized at $z_{\rm init} = 99$, with density perturbations drawn from the Eisenstein & Hu (1999) power spectrum. The initial density fluctuations are assumed equal for the baryons and dark matter, and the initial gas temperature is uniformly 110.7 K. The parameters of our runs (identified in order of increasing mass resolution as Very Low, Low, High, and Very High resolution) are shown in Table 1. In each case, we first run a low resolution dark matter only run, in which the simulation volume $l_{\rm root}^3$ is resolved on a 128^3 root grid. We include an additional $n_{\rm ref}$ static levels of refinement (listed in Table 1 for each run) inside this central cube. Furthermore, grid cells inside the central region are allowed to dynamically refine so that the Jeans length is resolved by at least 4 grid zones and no grid cell contains more than 4 times the initial gas mass element. Each additional grid level refines the mesh length of the parent grid cell by a factor of 2. We allow for a maximum of 11 levels of refinement inside the refined central region, granting us a spatial resolution of $l_{\rm root}/(128 \times 2^{11})$. The dark matter particle mass for each run is shown in Table 1. We also include the non-equilibrium reaction network of nine chemical species (H, H^+, He, He^+, He^{++}, e^-, H_2, H_2^+, H^-) using the algorithm of Anninos et al. (1997), and initialized with post-recombination abundances from Anninos & Norman (1996). Our analysis below is based on the central refined region; the low resolution dark matter outside the refined region serves to provide the necessary tidal forces to our refined region.

Each simulation includes two ionization scenarios: (1) no UV background radiation (hereafter "NoUV"), and (2) flash ionization at $z = 25$ ("Flash") which instantaneously sets the gas temperature to T=10,000 K and the hydrogen neutral fraction to $x_{\rm HI} = 10^{-3}$ throughout the simulation volume, but involves no heating thereafter.

We use the HOP algorithm (Eisenstein & Hut 1998) on the DM particles to identify DM halos. Since we are interested in the gas fraction, it is essential to sum up both the DM mass and the gas mass over the same volume. We obtain the total DM and baryonic mass of each halo by integrating the densities over a sphere whose radius is the halo's virial

radius[1]. Additionally, we discount halos which have been substantially contaminated by the large (low-resolution) DM particles outside of our refined region. Specifically, we remove from our analysis halos with an average DM particle mass greater than $\sim 130\%$ of the refined region's DM mass resolution.

The simulations do not attempt to model global reionization. Instead we focus on a short-lived UV background that can occur from a localized star formation episode. Specifically, the Flash scenario enabled Mesinger, Bryan & Haiman (2006) to compare their results to O'Shea et al. (2005a). and to check the importance of including additional dynamical effects of prolonged photoheating. For us, this is simply a good test case of a time-variable Jeans mass at high redshift.

3 THE RESOLUTION DEPENDENCE OF THE GAS FRACTION IN HALOS

Our simulation runs at four different resolutions (Table 1) allow us to carefully test the dependence of the gas fraction estimates on the resolution. We find that the halo gas fraction indeed varies strongly with the resolution. This can be seen in Figs. 1 and 2, which show the gas fraction in halos as a function of the halo mass. The gas fraction is shown for each of our runs, averaged over bins of halo mass. These figures show that the lower resolution runs underestimate the gas fraction at a given halo mass, often substantially. However, our two highest-resolution runs, Hres and VHres, agree in their gas fractions over essentially their entire halo mass range, and above that range (i.e., at $M \gtrsim 10^6 M_\odot$) the two lower resolution runs agree. This demonstrates numerical convergence and suggests that if we take our highest-resolution run at each halo mass, then we obtain the correct value of the mean halo gas fraction.

Getting a correct gas fraction in simulations is important in calculating, for example, the galaxy abundance. Underestimation of the gas fraction in halos can give incorrect results. The VLres run was used by Mesinger, Bryan & Haiman (2006) and at the time was considered a very high resolution run in the high-redshift regime. We find, however, that our high resolution runs (i.e., Hres and VHres) estimate the gas fraction in the NoUV case to be higher than for the VLres run by a factor of ~ 1.6 for a halo mass of $10^5 M_\odot$. Note, that Mesinger, Bryan & Haiman (2006) focus on whether the gas has cooled relative to other runs at the same resolution, not the exact amount of gas inside each halo. Furthermore, that study focused on halos whose gas was capable of cooling via the molecular hydrogen channel, corresponding to masses greater than $\sim 5 \times 10^5 M_\odot$ at these redshifts, where the gas fraction is beginning to converge to the higher-resolution values.

We can further quantify the resolution dependence of the halo gas fraction. At each halo mass, we adopt the gas fraction as given by our highest-resolution simulation available at that mass scale ($f_{g(\mathrm{Highest-res})}$) to be the correct value, and compare to this the result from all lower-resolution simulations that have halos of that same mass at the same redshift. We plot in Figure 3 these ratios, $f_g/f_{g(\mathrm{Highest-res})}$, where each simulation at each output redshift is compared to the highest-resolution run at the same halo mass and redshift. In order to test the idea that the resolution effect depends primarily on the halo mass resolution, these ratios are shown as a function not of the halo mass but of the number of particles in each halo (N_h) in the lower-resolution run. Note that for this we divided our various runs into the same mass bins. Now, if the halo gas fraction did not depend on resolution then we would simply get unity. Instead, the figure shows that the lower resolution runs underestimate the gas fractions in halos. In Figure 3 we show together all the various redshift outputs from all the different runs; all the redshift are consistent with a single relation, i.e., they agree quantitatively. Despite the scatter, there is a rather uniform trend among all the points (excluding the open circles in the Flash case – see below), confirming the idea that the resolution dependence is mainly an effect of halo mass resolution.

The gas fractions in some halos are less accurately determined in the Flash case, for a simple reason. In this scenario the global heating in the simulation evaporates the gas, i.e., the heating raises the characteristic mass (see also section 4). This is easily seen in Fig. 2, where we observe a declining gas fraction with time in the low-mass range (consistent with Haiman, Rees & Loeb 1997). Thus, the gas fraction in each halo is naturally more sensitive to the halo's surroundings and to numerical errors when the gas fraction is very low.

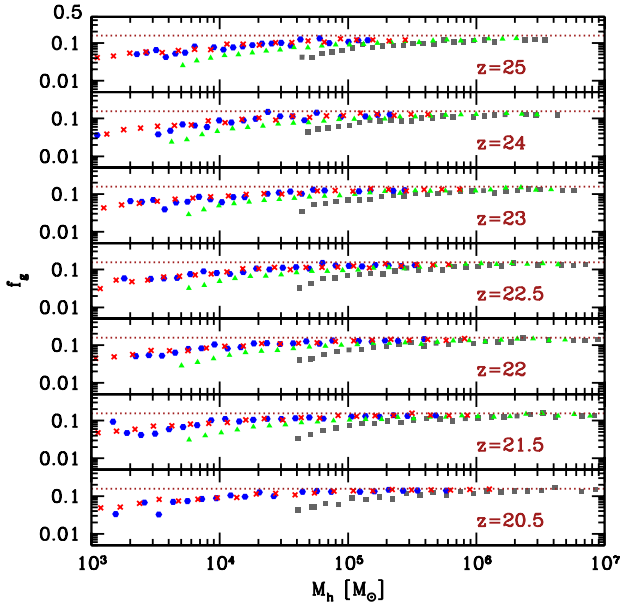

Figure 1. NoUV case: The halo gas fraction f_g as a function of the halo mass M_h in the simulations. We consider the following simulations runs: VLres (squares), Lres (triangles), Hres (crosses), and VHres (circles). Note that we did not use the Lres data at $z = 20.5$ because of a numerical error.

[1] We define the virial radius as the radius of the spherical volume within which the mean density is Δ_c times the critical density. Δ_c is obtained through the fitting formula in Bryan & Norman (1998) and is ~ 178 in an Einstein-DeSitter universe. We find that the halo masses thus obtained generally agree within a factor of two with masses obtained directly from the HOP algorithm assuming a mean baryon fraction.

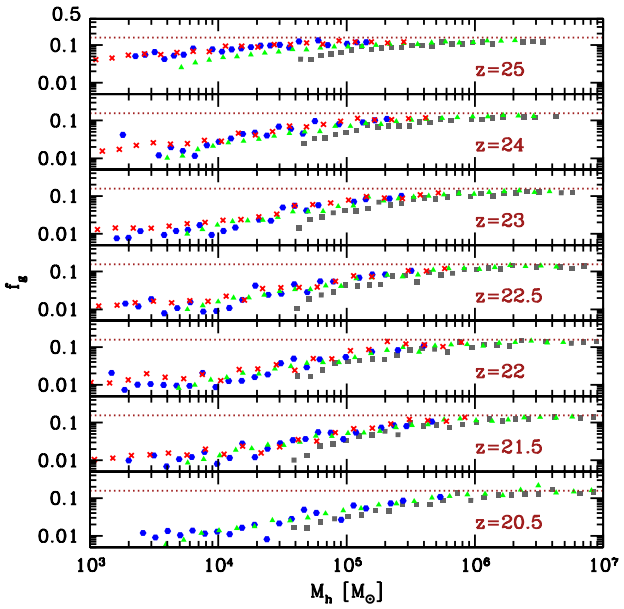

Figure 2. Flash case: The halo gas fraction f_g as a function of the halo mass M_h in the simulations. Same conventions as in Fig. 1. Note that we did not use the Hres data at $z = 20.5$ because of a numerical error.

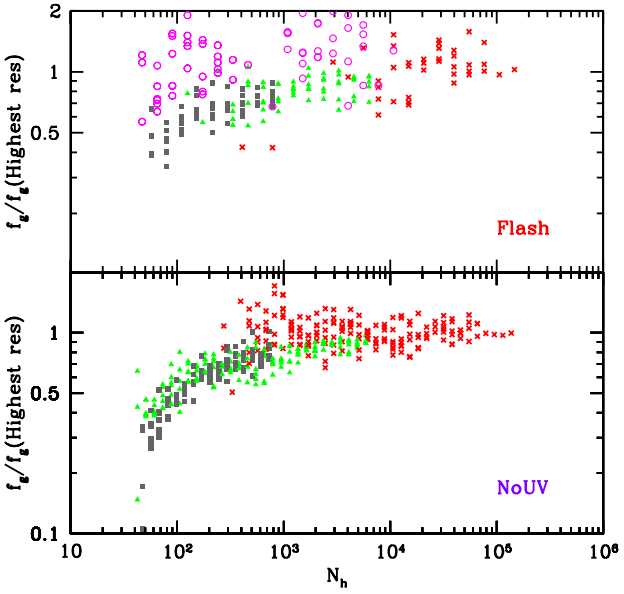

Figure 3. The ratio between the halo gas fraction in one simulation and the gas fraction in the highest-resolution run in the same mass bin, as a function of the number of particles per halo (N_h) in the lower-resolution run. We show these ratios from all the output redshifts. We consider the NoUV (bottom panel) and Flash (upper panel) cases, with symbols corresponding to the lower-resolution run using the same conventions as in Fig. 1. For the Flash case we only include halos for which $f_g > f_{g,min} = 0.03$ in the higher-resolution run (see text), and we separately show the results from the excluded halos (open circles).

Indeed, we find large scatter below $f_g \sim 0.03$, which corresponds to low-mass halos (below $M \sim 5 \times 10^4$ $M_\odot$) at redshifts well after the UV flash. We thus consider only the halos for which the gas fraction is larger than the fiducial value $f_{g,min} = 0.03$.[2] The upper panel of Fig. 3 confirms the need for this separation, showing that the Flash halos with $f_g > f_{g,min}$ follow a similar trend as the halos in the NoUV case, while the excluded halos with $f_g < f_{g,min}$ are inconsistent and show a much larger scatter.

To derive a useful result from Fig. 3, we first condense it efficiently by putting all the points together into a single set of bins in N_h. Specifically, we show in Fig. 4 one set of bins for the NoUV case, and one for the Flash case (including only the halos with $f_g > f_{g,min}$). This figure shows a clear trend, consistent between the two cases, of an artificially declining gas fraction in poorly resolved halos. If we desire a reasonably accurate determination of the mean halo gas fraction, with a systematic error of no more than 20% (i.e., $f_g/f_{g(\mathrm{Highest-res})} \geqslant 0.8$), then at least 500 particles per halo are required. For a 10% error, ~ 2000 particles are required per halo. On the other hand, halos resolved into only 100 particles underestimate the enclosed gas fraction by more than a factor of two. We adopt 500 as a minimum number, and henceforth consider only halos for which $N_h \geqslant 500$.

We note that, averaged over the output redshifts, the number of halos that we extract from each simulation is 104, 1532, 2479, and 2304, for the NoUV case and 102, 1641, 2601, and 324 for the Flash case, for the VLres, Lres, Hres, and VHres simulation, respectively. We also note that at redshift 20.5 we did not use the data for the simulation Lres for the NoUV case and Hres for the Flash case, due to numerical problems in these particular outputs. It is important to point out that we only performed this resolution test with Enzo. Although gas properties in dense regions are found to agree well in AMR and SPH cosmological simulations, different gravity solvers can lead to non-negligible differences in the N-body mass function at low masses (O'Shea et al. 2005a). Specifically, it seems that the gravitational softening in Enzo causes small halos to form somewhat late, but detailed resolution tests show that the halo gas fractions at a given time are unaffected by softening at least down to 100-particle halos (see Figure 14 in O'Shea et al. 2005b).

4 THE CHARACTERISTIC MASS AT HIGH REDSHIFT

4.1 Definition and relation to linear model

In linear theory the filtering mass, first defined by Gnedin & Hui (1998), describes the highest mass scale on which the baryon density fluctuations are suppressed significantly compared to the dark matter fluctuations. In Naoz & Barkana (2007) we included the fact that the baryons have smoother initial conditions than the dark matter (see Naoz & Barkana 2005) and found a lower value of the filtering mass (by a factor of 3−10, depending on the redshift). Following Naoz & Barkana (2007), the filtering scale

[2] We make this separation only in this resolution analysis, while in section 4 we calculate the scatter in each mass bin.

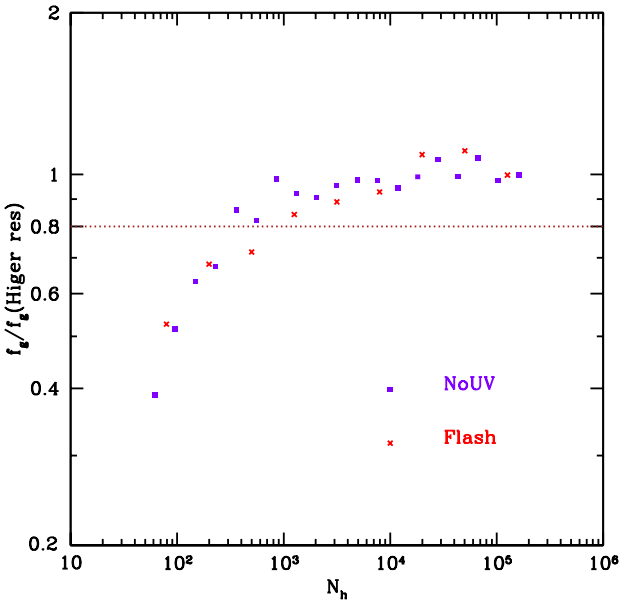

Figure 4. The ratio between the halo gas fraction in one simulation and the gas fraction in the highest-resolution run in the same mass bin, as a function of the number of particles per halo (N_h) in the lower-resolution run. We consider the NoUV case (squares) and the Flash case (circles), where in each case all the points from the various runs and output redshifts shown in Fig. 3 have been condensed into a single set of bins. In the Flash case we include only halos for which $f_g > f_{g,min} = 0.03$ in the higher-resolution run.

(specifically, the filtering wavenumber k_F) is defined by expanding the ratio of baryonic to total density fluctuations to first order in k^2:

$$\frac{\delta_{\rm b}}{\delta_{\rm tot}} = 1 - \frac{k^2}{k_F^2} + r_{\rm LSS} \ , \qquad (1)$$

where k is the wavenumber, and $\delta_{\rm b}$ and $\delta_{\rm tot}$ are the baryonic and the total (i.e., including both baryons and dark matter) density fluctuations, respectively. The parameter $r_{\rm LSS}$ (a negative quantity) describes the relative difference between $\delta_{\rm b}$ and $\delta_{\rm tot}$ on large scales (for more details see Naoz & Barkana 2007). The filtering mass is defined from k_F simply as:

$$M_F = \frac{4\pi}{3}\bar{\rho}_0 \left(\frac{1}{2}\frac{2\pi}{k_F}\right)^3 \ , \qquad (2)$$

where $\bar{\rho}_0$ is the mean matter density today. This relation is one eighth of the definition in Gnedin (2000) (based on a non-standard definition of the Jeans mass used there). Following Naoz & Barkana (2007) we calculate the filtering mass for the cosmological parameters assumed in this paper.

There is no apriori reason to think that the filtering mass can also accurately describe properties of highly nonlinear, virialized objects. For halos, Gnedin (2000) defined a characteristic mass M_c for which a halo contains half the mean cosmic baryon fraction f_b. In his simulation he found the mean gas fraction in halos of a given total mass M, and fitted the simulation results to the following formula:

$$f_{g,\rm calc} = f_{\rm b,0}\left[1 + \left(2^{\alpha/3} - 1\right)\left(\frac{M_c}{M}\right)^{\alpha}\right]^{-3/\alpha} \ , \qquad (3)$$

where $f_{\rm b,0}$ is the gas fraction in the high-mass limit. In this function, a higher α causes a sharper transition between the high-mass (constant f_g) limit and the low-mass limit (assumed to be $f_g \propto M^3$). Gnedin (2000) found a good fit for $\alpha = 1$, with a characteristic mass that in fact equaled the filtering mass by his definition. By our definition in eq. (2), the claim from Gnedin (2000) is that $M_c = 8 \times M_F$.

Recently, Hoeft et al. (2006) and Okamoto, Gao, & Theuns (2008) used higher resolution simulations than in Gnedin (2000) and showed that this claim is incorrect in the low-redshift regime. They compared the characteristic mass found in their simulations to the Gnedin & Hui (1998) filtering mass and found that the two values diverge after reionization. Specifically, they found that $\alpha = 2$ and $M_c(z = 0) \sim 6.5 \times 10^9$ $\rm M_\odot/\mathit{h}$, which is much lower than the filtering mass (and thus even lower compared to $8 \times M_F$). We caution that unlike our simple test cases, the heating in reionization simulations is complex and inhomogeneous, and thus the filtering mass cannot be directly and precisely defined and computed. Also note that the precise quantitative results during and after reionization depend on the thermal history of the gas which observationally is not well constrained, though results at $z = 0$ are more robust, as the gas in overdensities around halos has had more time to "forget" the details of its heating history. Nevertheless, by simulating a large set of thermal histories in a cosmological setting, Mesinger & Dijkstra (2008) were able to draw a general conclusion that the characteristic mass towards the end of reionization is likely in all cases to be close to the atomic-cooling threshold of $\sim 10^8 M_\odot$.

4.2 Simulation results

In order to determine the characteristic mass from our simulations, we put together the gas fraction measurements from all the simulation runs at each redshift, but including only the well-resolved halos, i.e., those with $N_h \geqslant 500$, as determined in section 3. We fit the simulation results to equation (3) with two free parameters, M_c and α, taking $f_{\rm b,0}$ to be the average gas fraction in the highest few mass bins[3]. We used a minimum-χ^2 method to estimate the best fit to equation (3) and to find the errors. To account for the numerical scatter we fitted this equation to the binned data, adopting the standard deviation within the mass bin as the uncertainty in each binned value. The best-fit parameters for both the NoUV and the Flash scenarios along with their 1-σ confidence limits are listed in Table 2 (and also shown in Fig. 7, which is discussed below). We also compare the binned data to the corresponding best fits in the form of eq. (3) in Figure 5.

Hoeft et al. (2006) and Okamoto, Gao, & Theuns (2008) found that the fits to their simulations were con-

[3] We note that we also tried to carry out the analysis with $f_{\rm b,0}$ assumed to be the cosmic mean value. This gave a substantially worse fit, with the parameters changed significantly ($\sim 40\%$ and $\sim 10\%$ changes in M_c and α, respectively). We also tried the approach of taking $f_{\rm b,0}$ to be a free parameter (in the NoUV case). This made less of a difference compared to taking $f_{\rm b,0}$ from the highest few mass bins. We found a lower M_c by $< 10\%$, a lower α by $< 6\%$, and a fitted value for $f_{\rm b,0}$ higher by $< 7\%$ than the simple estimate we used in the text.

Table 2. The best-fit parameters from equation (3).

Redshift	M_c [10^3 M$_\odot$]	α	reduced χ^2	degrees of freedom
		NoUV		
20.5	$4.52^{+1.45}_{-1.88}$	$0.47^{+0.06}_{-0.07}$	1.15	32
21.5	$3.28^{+0.79}_{-0.99}$	$0.41^{+0.03}_{-0.03}$	0.81	52
22	$5.65^{+0.17}_{-0.47}$	$0.70^{+0.01}_{-0.03}$	1.3	49
22.5	$4.43^{+0.64}_{-0.93}$	$0.53^{+0.04}_{0.05}$	0.54	46
23	$4.83^{+0.16}_{-0.16}$	$0.63^{+0.02}_{-0.02}$	1.4	35
24	$3.13^{+0.49}_{-0.47}$	$0.75^{+0.21}_{-0.11}$	0.45	33
25	$4.12^{+0.69}_{-1.42}$	$0.64^{+0.06}_{-0.1}$	0.21	21
		Flash		
20.5	$141.3^{+11.0}_{-12.8}$	$0.49^{+0.02}_{-0.02}$	0.9	31
21.5	$68.7^{+0.1}_{-1.41}$	$0.64^{+0.01}_{-0.01}$	1.6	48
22	$51.47^{+5.67}_{-5.25}$	$0.48^{+0.02}_{-0.02}$	3.8	54
22.5	$55.99^{+0.27}_{-1.23}$	$0.63^{+0.01}_{-0.01}$	1.58	53
23	$22.83^{+2.46}_{-2.43}$	$0.62^{+0.03}_{-0.03}$	0.85	36
24	$16.2^{+3.4}_{-0.6}$	$0.72^{+0.07}_{-0.07}$	0.96	31
25	$4.12^{+0.69}_{-1.42}$	$0.64^{+0.06}_{-0.1}$	0.17	26

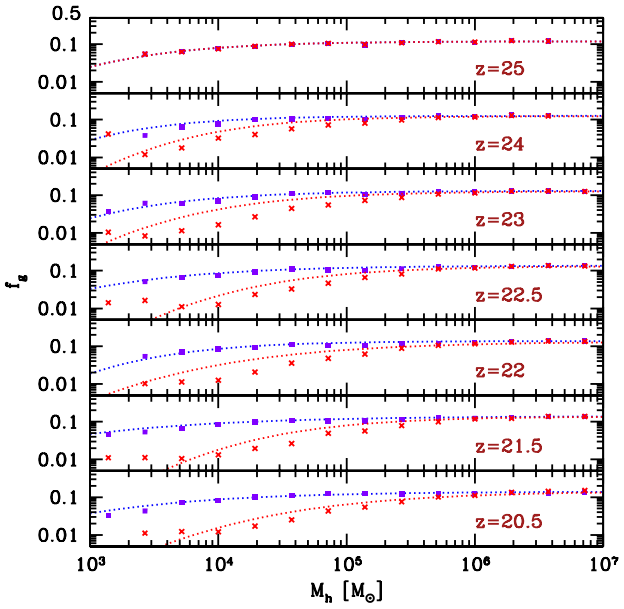

Figure 5. The gas fraction in all the simulations vs. the halo mass at various redshifts. The simulation data have been binned by halo mass. We use only data points from halos with $N_h \geqslant 500$. We consider the Flash (crosses) and NoUV (filled squares) cases. Also shown are the best fits in each case in the form of eq. (3). We note that the bins show here are equally spaced for representations reasons, for the actual degrees of freedom see table 2.

sistent with $\alpha = 2$. However, we find that our fits yield $\alpha \sim 0.4 - 0.7$ (see Table 2 and also Fig. 7 middle panel). In Figure 6 we show the dependence of the reduced χ^2 on the fit parameters M_c and α at $z = 20.5$. This figure shows that a low α gives the best fit to equation (3), and suggests that

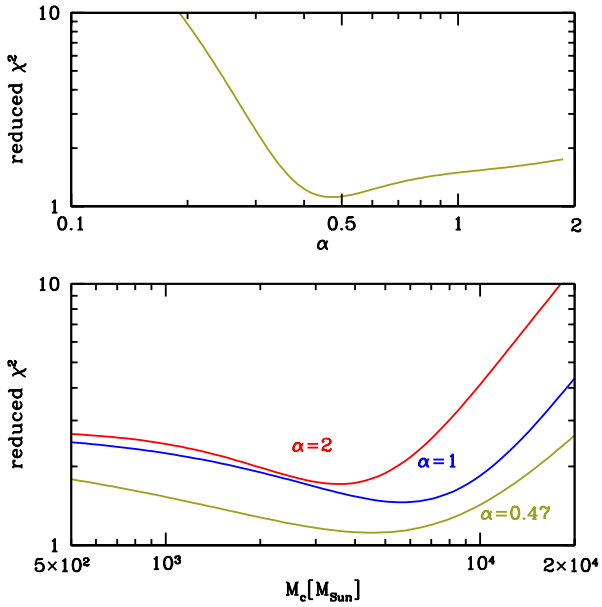

Figure 6. The dependence of the reduced χ^2 on the parameters of the fit at $z = 20.5$. There are 33 degrees of freedom in this case. Bottom panel: dependence on M_c obtained while fixing $\alpha = 2$, 1, or 0.47, from top to bottom respectively, where the lowest value is the best-fit one (see table 2). Upper panel: dependence on α, fixing the best-fit value $M_c = 4.52 \times 10^3$ M$_\odot$.

the characteristic mass scale found assuming $\alpha = 2$ would be an underestimate by about 15% in this case.

Figure 7 shows the best fitted parameters at various redshifts for M_c and α, and our value for $f_{\rm b,0}$, for both the NoUV and Flash scenarios. The 1-σ (68%) confidence regions are listed in table 2; since these statistical errors are small, we do not show them in the figure. Indeed, particularly in the Flash case, the fits do not drop as quickly as the data points do towards low halo masses, and so tend to systematically underestimate the characteristic mass. Thus, to obtain a more realistic estimate of the systematic error resulting from the form of the fit, we also show M_c as derived directly from the binned data without a fit; in this case we simply found the maximum halo mass for which $f_g = f_{\rm b,0}/2$ (interpolating inbetween the binned points). We find that the systematic errors for the NoUV case (typical difference of a factor of 1.5–2 between the fit and the no-fit values) are substantially smaller than in the Flash case (typical difference of a factor of 3), and they are much larger than the statistical errors in both cases.

Figure 7 also shows the analytical calculation from linear theory of the filtering mass, as described in detail in Naoz & Barkana (2007); we make this calculation for both the NoUV and Flash scenarios, assuming the same initial conditions as in the simulations. As mentioned above, the simulation assumes equal baryon and dark matter fluctuations at its $z_{\rm init} = 99$ (as is commonly assumed in the literature), while the correct baryonic initial conditions are smoother (see below). Note that due to the simplicity of the Flash scenario that we have implemented in the simulation, we can easily incorporate it precisely within the analytical calculation. We also directly tested the effect of radiative

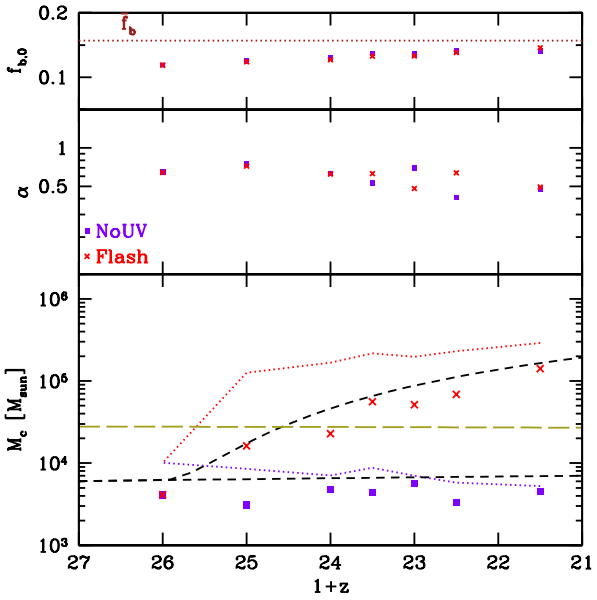

Figure 7. The parameters of the best fits in the form of equation 3; different panels show M_c, α, and $f_{\rm b,0}$. We consider the Flash (crosses) and NoUV (filled squares) cases, where we fit equation 3 to all data points from halos with $N_h \geqslant 500$. For comparison we also show the M_c values derived directly from interpolating the binned data, without assuming a fitting function (dotted curves in the bottom panel; bottom: NoUV, top: Flash scenario). In the bottom panel we also show the analytical calculation according to Naoz & Barkana (2007), assuming the same initial conditions as in the simulations (short-dashed curves; bottom: NoUV, top: Flash). The full calculation assuming the true initial conditions as in Naoz & Barkana (2007) is also shown for the NoUV case (long-dashed curve). We note that the NoUV and Flash cases mostly overlap in the top panel, which also shows the cosmic mean baryon fraction (horizontal dotted line).

cooling, which is included in the simulations but not the analytical model. We carried out an additional Flash run with a resolution identical to that of the Hres run, but where the radiative cooling was eliminated, leaving only adiabatic cooling and Compton heating. We found that the gas fractions (and thus the fitted characteristic mass) did not change significantly, and thus verified that radiative cooling has a negligible effect on our results.

We find that, given our systematic errors, the filtering mass from linear theory is consistent with the characteristic mass fitted from the simulations for both the NoUV and the Flash cases[4]. It is important to emphasize that in this statement we are referring to our definition in equation (2), which is one eighth of the original definition which Gnedin (2000) claimed was a good fit to the characteristic mass. In any case, we conclude that at least in a particular redshift range ($z = 20 - 25$) the filtering mass provides a fairly good estimate to the characteristic mass, either before stellar heating or in its initial stages. Since we have not probed a larger range of redshifts, we cannot generalize this conclusion. Also, the large systematic errors (particularly in the Flash case) reduce the significance of the above conclusion.

In Figure 7 we also show the filtering mass from the full calculation of Naoz & Barkana (2007) assuming the correct initial conditions (see figure 1 of Naoz & Barkana 2005), in the NoUV case. The correct initial conditions cannot be fully directly incorporated in a simulation without starting at much higher redshifts than simulators are used to. In particular, these initial conditions include the fact that at $z = 1200$ the baryons are still essentially uniform (on scales relevant for galactic halos) due to their just ended strong coupling to the CMB photons. Based on the agreement we have found between the linear theory and the simulations for the case of the simulations' initial conditions, we suggest that we can estimate the real characteristic mass in the universe based on our analytical filtering mass calculation with the true initial conditions.

There are several differences between our simulations' initial conditions and the true ones. The initial conditions in the simulations assumed a lower temperature (by $\sim 30\%$ at $z_{\rm init} = 99$) than the exact calculation with Compton heating, resulting in lower gas pressure and thus a lower filtering mass than in the full analytical calculation. The assumption that the baryon perturbations follow the dark matter at $z_{\rm init} = 99$ creates tendencies to both raise the filtering mass (since the baryon fraction, and thus the gas pressure, is too high within perturbations) and lower it (since the filtering mass reflectes the integrated effect of pressure, and the integral is only begun at $z_{\rm init} = 99$ instead of at $z = 1200$). Also, we note that the best-known cosmological parameters are slightly different from those in our simulation, i.e., in our analytical calculation we use those of Spergel et al. (2007): (Ω_Λ, $\Omega_{\rm M}$, Ω_b, n, σ_8, H_0) = (0.701, 0.299, 0.0478, 0.957, 0.82, 68.7 km s^{-1} Mpc^{-1}). However, changing the cosmological parameters does not play an important role. This is because the definition of the filtering mass is independent of σ_8 which is the major difference in the cosmological parameters. Thus, we conclude that the true minimum mass needed for a halo to keep at least half of its baryons, in the era before stellar heating (i.e., corresponding to the NoUV case), is about 2.7×10^4 M$_\odot$ at $z \sim 20 - 25$.

Finally, we can also use our simulations to look beyond the tight $f_g(M)$ relation of equation (3), and consider the distribution of gas fractions for a given halo mass. Gnedin (2000) showed that this distribution in the simulation is well approximated as a lognormal distribution. Performing the same analysis for the NoUV scenario, we find the same, as shown in Figure 8. Since we have a limited number of halos, we collect all of our data at each redshift and consider the ratio between the measured f_g and that predicted by equation (3) with the best-fit parameters. Thus, we assume that this relative distribution does not vary strongly with halo mass. Since it is easier to deal with a normal distribution, we plot the distribution of $\ln(f_g/f_{g,\rm calc})$ and fit to it a normal distribution with mean μ and standard deviation σ. We show the best-fit parameter values with their 1-σ confidence ranges in Table 3.

[4] We note that equation (3) is successful in giving a reduced $\chi 2$ of order unity in all cases except one (see Table 2).

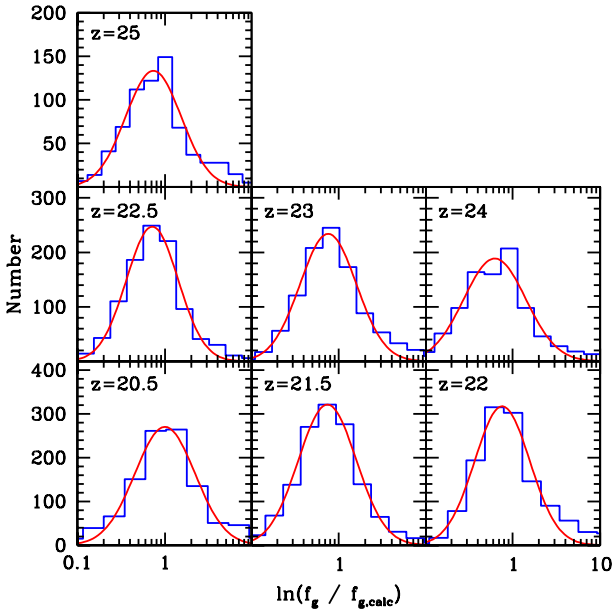

Figure 8. The distribution of gas fractions with respect to the prediction of equation (3). The histograms show the binned data of $\ln(f_g/f_{g,\rm calc})$, where $f_{g,\rm calc}$ for each halo mass is taken from eq. (3) assuming the best-fit parameters as given in Table 2. We also show in each case the best fit to a normal distribution (solid curves).

Table 3. The parameters of the best-fit normal distributions to the histograms shown in Figure 8.

redshift	μ	σ	reduced χ^2
20.5	0.0003 ± 0.015	0.24 ± 0.01	0.98
21.5	-0.14 ± 0.014	0.22 ± 0.01	0.99
22	-0.12 ± 0.01	0.22 ± 0.01	0.97
22.5	-0.14 ± 0.01	0.21 ± 0.006	0.99
23	-0.12 ± 0.01	0.24 ± 0.009	0.98
24	-0.20 ± 0.02	0.24 ± 0.01	0.96
25	-0.13 ± 0.02	0.22 ± 0.01	0.93

5 CONCLUSIONS

We have used three-dimensional hydrodynamic simulations to investigate the resolution requirements needed to determine correctly the gas fraction in halos in the early universe. We considered both a NoUV case with no stellar heating, and a Flash case with instantaneous stellar heating. We found that the gas fraction in halos is strongly dependent on the mass resolution of the simulation (see Figs. 1 and 2) both in the NoUV and Flash cases. Using our multiple runs at various resolutions, we demonstrated convergence in the estimated gas fractions over a wide range of halo masses; thus we concluded that these estimates are likely correct. Comparing these converged values to the results from lower-resolution simulations, we showed (see Figs. 3 and 4) that halos that are poorly resolved (in terms of the number of dark matter particles) yield artificially low gas fractions. In particular, we concluded that to ensure a gas fraction that is unbiased to $< 20\%$, there must be at least 500 particles in each halo (and 2000 particles for $< 10\%$ bias). We showed that such a simple condition is a consistent description of the resolution dependence over the full range of redshifts and heating stages that we investigated.

We found from the simulations the characteristic mass scale below which a halo does not contain most of its baryons and can be considered "gas poor". Specifically, we fitted eq. (3) to the data from the simulations with two parameters, the characteristic mass M_c and α. We found that they are roughly constant with redshift for the NoUV case (see Fig. 5 for the fit, also Fig. 7 and table 2 for the best fit parameters). We compared between the simulations' characteristic mass and the analytical filtering mass, using the simulations (with their particular initial conditions) as case studies. We found that the M_c estimations from the simulations are consistent with the filtering mass from linear theory, according to our definition which is one eighth of the definition that Gnedin (2000) claimed was a good fit to the characteristic mass. Due to our limited redshift range and fairly large systematic errors, we cannot be sure how general this consistency may be. We note that this agreement between the simulations and the linear theory in the NoUV and the Flash scenarios occurred in a regime where the heating is simple and easily incorporated within linear theory. In more complicated situations with inhomogeneous heating from astrophysical sources, the filtering mass cannot be directly and precisely computed, and this may explain apparent inconsistencies between the theory and simulations (Hoeft et al. 2006; Okamoto, Gao, & Theuns 2008). Note that these authors used the Gnedin (2000) definition for the filtering mass, which is eight times our definition.

The agreement between the linear calculation of the filtering mass and the simulations suggests that using the correct initial conditions we can calculate the true minimum mass in the real universe for which a halo keeps most of its gas during its formation. We calculated the filtering mass using the correct initial conditions starting from very high redshift (see, Naoz & Barkana 2005), finding a characteristic mass of 2.7×10^4 $M_\odot$ assuming no stellar heating prior to $z \sim 20$. (see Fig. 7). We note that the filtering mass for the Flash scenario with true initial conditions would have to be corrected by approximately the same factor as M_c in the NoUV case; we did not show this curve in Fig. 7 to avoid a busy figure.

As noted in the introduction, minihalos can have important, observable effects, in particular on the early stages of cosmic reionization. We have taken an important step towards understanding the importance of minihalos by establishing which ones contain substantial amounts of gas. Also, since the minimum mass for molecular hydrogen cooling is $\sim 10^5 M_\odot$, somewhat higher than the characteristic mass for minihalos, we conclude that the gas fraction within the host halos of the first stars could be slightly (though probably not greatly) reduced compared to that of more massive halos; this effect is likely missing or quantitatively inaccurate in many simulations of the first stars, due to their inability to start with the correct initial conditions at sufficiently high initial redshifts.

ACKNOWLEDGMENTS

We wish to thank Greg Bryan for helpful conversations and comments on the paper. SN and RB acknowledge support by Israel Science Foundation grant 629/05 and U.S. - Israel Binational Science Foundation grant 2004386. RB is grateful for support from the Moore Distinguished Scholar program at Caltech and the John Simon Guggenheim Memorial Foundation. SN also acknowledges the support of the John Bahcall Graduate Student Prize. Support for this work was also partially provided by NASA through Hubble Fellowship grant #HF-01222.01 to AM, awarded by the Space Telescope Science Institute, which is operated by the Association of Universities for Research in Astronomy, Inc., for NASA, under contract NAS 5-26555. We also acknowledge computational support from the National Center for Supercomputing Applications.

REFERENCES

Abel T., Anninos P., Zhang Y., Norman M. L., 1997, NewA, 2, 181
Abel T., Bryan G. L., Norman M. L., 2002, Sci, 295, 93
Anninos P., Norman M. L., 1996, ApJ, 460, 556
Anninos P., Zhang Y., Abel T., Norman M. L., 1997, NewA, 2, 209
Barkana R., Loeb A., 1999, ApJ, 523, 54
Barkana, R., & Loeb, A. 2001, Phys. Rep., 349, 125
Barkana R., Loeb A., 2002, ApJ, 578, 1
Barkana R., Loeb A., 2005, MNRAS, 363, L36
Benson A. J., Frenk C. S., Lacey C. G., Baugh C. M., Cole S., 2002a, MNRAS, 333, 177
Benson A. J., Lacey C. G., Baugh C. M., Cole S., Frenk C. S., 2002b, MNRAS, 333, 156
Bromm V., Coppi P. S., Larson R. B., 2002, ApJ, 564, 23
Bromm V., Coppi P. S., Larson R. B., 1999, ApJ, 527, L5
Bromm V., Loeb A., 2004, NewA, 9, 353
Bullock J. S., Kravtsov A. V., Weinberg D. H., 2000, ApJ, 539, 517
Bryan G. L., 1999, CoScE, 1, 46
Bryan G. L., Norman M. L., 1998, ApJ, 495, 80
Cen R., 2003, ApJ, 591, L5
Dijkstra M., Haiman Z., Rees M. J., Weinberg D. H., 2004, ApJ, 601, 666
Dunkley J., et al., 2008, arXiv, arXiv:0811.4280
Efstathiou G., 1992, MNRAS, 256, 43P
Eisenstein D. J., Hu W., 1999, ApJ, 511, 5
Eisenstein D. J., Hut P., 1998, ApJ, 498, 137
Fuller T. M., Couchman H. M. P., 2000, ApJ, 544, 6
Furlanetto S. R., Oh S. P., 2006, ApJ, 652, 849
Gnedin, N. Y. & Hui, L. 2004, MNRAS, 296.
Gnedin N. Y., 2000, ApJ, 542, 535.
Haiman Z., Holder G. P., 2003, ApJ, 595, 1
Haiman, Z., Rees, M. J. & Loeb, 1997, ApJ, 476.
Helly J. C., Cole S., Frenk C. S., Baugh C. M., Benson A., Lacey C., Pearce F. R., 2003, MNRAS, 338, 913
Hoeft M., Yepes G., Gottlöber S., Springel V., 2006, MNRAS, 371, 401
Hui L., Gnedin N. Y., 1997, MNRAS, 292, 27
Iliev, I. T., Scannapieco, E., Martel, H., & Shapiro, P. R. 2003, MNRAS, 341, 81
Iliev I. T., Scannapieco E., Shapiro P. R., 2005, ApJ, 624, 491
Jeans, J. H. Cambridge University press, (1928).
Kitayama T., Ikeuchi S., 2000, ApJ, 529, 615
Kuhlen M., Madau P., Montgomery R., 2006, ApJ, 637, L1
Ma C., Bertschinger E., 1995, ApJ, 455, 7
McQuinn M., Lidz A., Zahn O., Dutta S., Hernquist L., Zaldarriaga M., 2007, MNRAS, 377, 1043
Mesinger A., Bryan G., & Haiman Z. 2006, ApJ, 648, 835
Mesinger A., Bryan G. L., Haiman Z., 2008, arXiv, arXiv:0812.2479
Mesinger A., Dijkstra M., 2008, MNRAS, 390, 1071
Mesinger A., Johnson B. D., Haiman Z., 2006, ApJ, 637, 80
Nagashima M., Gouda N., Sugiura N., 1999, MNRAS, 305, 449
Naoz S., Barkana R., 2005, MNRAS, 362, 1047
Naoz S., Noter S., Barkana R., 2006, MNRAS, 373, L98
Naoz S., Barkana R., 2007, MNRAS, 377, 667
Naoz S., Barkana R., 2008, MNRAS, 385, L63
Navarro J. F., Frenk C. S., White S. D. M., 1997, ApJ, 490, 493
Norman M. L., Bryan G. L., 1999, ASSL, 240, 19
Okamoto T., Gao L., Theuns T., 2008, arXiv, 806, arXiv:0806.0378
O'Shea B. W., Abel T., Whalen D., Norman M. L., 2005, ApJ, 628, L5
O'Shea B. W., Abel T., Whalen D., Norman M. L., 2005, ApJS, 169, 1
Peebles P. J. E., 1980, The Large-Scale Structure of the Universe, Princeton Univ. Press, Princeton
Press W. H., Schechter P., 1974, ApJ, 187, 425
Quinn T., Katz N., Efstathiou G., 1996, MNRAS, 278, L49
Sheth R. K., Mo H. J., Tormen G., 2001 ,MNRAS, 323, 1
Sheth R. K., Tormen G., 2002, MNRAS, 329, 61
Shapiro P. R., Ahn K., Alvarez M. A., Iliev I. T., Martel H., Ryu D., 2006, ApJ, 646, 681
Shapiro P. R., Giroux M. L., Babul A., 1994, ApJ, 427, 25
Somerville R. S., 2002, ApJ, 572, L23
Springel V., Hernquist L., 2003, MNRAS, 339, 312
Spergel D. N., et al., 2007, ApJS, 170, 377
Tegmark M., et al., 1997, ApJ, 474, L77
Thoul A. A., Weinberg D. H., 1996, ApJ, 465, 608
Trenti M., Stiavelli M., 2009, arXiv, arXiv:0901.0711
Wyithe J. S. B., Loeb A., 2003, ApJ, 588, L69
Yoshida N., 2005, PThPS, 158, 117